Journal Pre-proofs

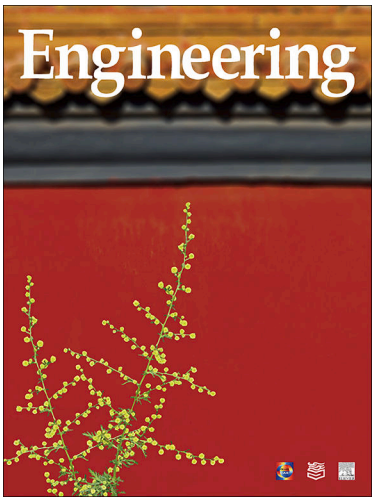

Article

Synergistic Effects of Fuel Stratification and Preferential Diffusion for Ultra-Low NO*x* Formation in Hydrogen Flames

Tianze Yu, Long Zhang, Hua Zhou, Zhuyin Ren, Xiaohua Gan

PII: S2095-8099(26)00068-8
DOI: https://doi.org/10.1016/j.eng.2026.01.023
Reference: ENG 2245

To appear in: *Engineering*

Received Date: 23 March 2025
Revised Date: 17 January 2026
Accepted Date: 20 January 2026

Please cite this article as: T. Yu, L. Zhang, H. Zhou, Z. Ren, X. Gan, Synergistic Effects of Fuel Stratification and Preferential Diffusion for Ultra-Low NO*x* Formation in Hydrogen Flames, *Engineering* (2026), doi: https://doi.org/10.1016/j.eng.2026.01.023

This is a PDF of an article that has undergone enhancements after acceptance, such as the addition of a cover page and metadata, and formatting for readability. This version will undergo additional copyediting, typesetting and review before it is published in its final form. As such, this version is no longer the Accepted Manuscript, but it is not yet the definitive Version of Record; we are providing this early version to give early visibility of the article. Please note that Elsevier's sharing policy for the Published Journal Article applies to this version, see: https://www.elsevier.com/about/policies-and-standards/sharing#4-published-journal-article. Please also note that, during the production process, errors may be discovered which could affect the content, and all legal disclaimers that apply to the journal pertain.

© 2026 THE AUTHORS. Published by Elsevier LTD on behalf of Chinese Academy of Engineering and Higher Education Press Limited Company.

Mechanical Engineering—Article

Synergistic Effects of Fuel Stratification and Preferential Diffusion for Ultra-Low NO*x* Formation in Hydrogen Flames

Tianze Yu, Long Zhang, Hua Zhou, Zhuyin Ren *, Xiaohua Gan

Institute for Aero Engine, Tsinghua University, Beijing 100084, China

* Corresponding author.

E-mail address: zhuyinren@tsinghua.edu.cn (Z. Ren).

Abstract: The unique transport properties of hydrogen give rise to fuel re-stratification and super-adiabatic flame temperature (SAFT) in premixed flames—phenomena that are generally not absent in fossil-fuel combustion. These effects undermine the effectiveness of conventional fuel/air fully premixed technology for achieving low NO*x* emissions in hydrogen energy and propulsion systems. In this study, a scaling law for SAFT, incorporating the Lewis number (*Le*) and Zel'dovich number (*Ze*), is revisited for fully premixed hydrogen laminar flames under flow straining conditions. The impact of SAFT on NO*x* formation, with particular emphasis on thermal NO*x* governed by the Zel'dovich mechanism, is systematically analyzed. A theoretical expression is derived to estimate the thermal NO*x* reaction rate as a function of SAFT. With these new insights, a novel concept based on the synergistic effects of fuel stratification and preferential diffusion is proposed to achieve ultra-low NO*x* emissions in hydrogen combustion. The effectiveness of this concept is demonstrated in multi-slot flames, where a designed nonuniform equivalence ratio (ϕ) at the inlet configuration reduces peak temperature by 53–236 K and NO emissions by 15%–54% over the typical gas-turbine operating range of $0.4 < \phi < 0.7$, compared with a fully premixed inlet configuration. This counter-intuitive approach provides new insights into hydrogen flame control and offers a promising pathway to achieving ultra-low NO*x* emissions in hydrogen energy and propulsion systems.

Keywords: Zero carbon emission; Hydrogen flames; Fuel stratification; Preferential diffusion; NO*x* emission

1. Introduction

The global push toward Net Zero Emissions [1] has accelerated the deployment of renewable energy sources such as wind and solar power. However, the inherently intermittent nature of these resources leads to fluctuations in electricity supply, necessitating reliable, affordable, and sustainable dispatchable power generation. Hydrogen gas turbines represent a promising solution for providing clean and reliable electricity [2,3], owing to their dispatchable capability and compatibility with emerging hydrogen infrastructure. Consequently, considerable research efforts have been devoted to hydrogen flame dynamics [4,5] and instability [6,7].

Although hydrogen gas turbines produce zero carbon emissions, NO*x* formation remains unavoidable due to the presence of nitrogen in the combustion process. Lean premixed combustion is generally an effective strategy for NO*x* mitigation, as reduced flame temperatures significantly suppress the thermal NO*x* pathway. However, in hydrogen flames, flame stretching can induce super-adiabatic flame temperature (SAFT), whereby the local temperature exceeds the adiabatic flame temperature as a result of differential diffusion arising from disparities in species and thermal diffusivity. Hydrogen's exceptionally high mass diffusivity amplifies this effect, with previous studies reporting flame temperature exceeding the adiabatic flame temperature by more than 20% [8]. Recent studies have extensively investigated SAFT phenomena. Wang et al. [9] reproduced similar SAFT behavior observed in direct numerical simulation (DNS) of turbulent premixed jet flames using the transport probability density function method. Experimental investigation by Shi et al. [10] on piloted turbulent jet burners reported SAFT values up to 160 K above the adiabatic flame temperature. In addition, Zhang et al. [11,12] demonstrate that hydrogen enrichment in hydrocarbon fuels significantly impacts laminar flame speed; in particular, differential diffusion effects in rich hydrogen flames lower the predicted flashback speed by more than 30%. Collectively, these distinctive combustion characteristics, which differ markedly from those of natural gas, underscore the need to revisit the fundamental properties of hydrogen and to develop advanced combustion technologies capable of achieving ultra-low emissions.

Journal Pre-proofs

The theoretical foundations of transport characteristics in premixed flames date back to the 1980s. Matalon and [illegible] al diffusion effect, characterized by the Lewis number, in stretched flames using the method of matched asymptotic expansions. Chung and Law [14] obtained similar results using an approximate integral approach and further investigated the nonlinear response of stretched premixed flames across different geometries [14–16]. In the 21st century, research has increasingly focused on molecular transport effects in turbulent flames. Day et al. [17] demonstrated that localized hot spots induced by the preferential diffusion of hydrogen significantly enhance NO formation, even when peak temperatures remain below 1800 K. More recently, Wen et al. [18] quantified the effects of flame curvature on NO*x* formation pathways using DNS in a sufficiently large three-dimensional computational domain. Vance and Scholtissek [19] indicated that non-uniform equivalence ratio distribution can reduce flashback risk, while Lipatnikov [20] demonstrated that fuel stratification promotes a back-supported flame structure with distinct propagation characteristics, enhancing stability in jet flame configurations. Collectively, these findings indicate that properly designed non-uniform fuel distribution can offer several safety-related benefits in gas turbine combustors. Despite these advances, studies examining the synergistic effects of fuel stratification and preferential diffusion on NO*x* emissions in practical hydrogen combustion configurations remain limited, motivating the present work.

This study begins by examining the unique transport properties of hydrogen, which give rise to two key phenomena: SAFT and fuel re-stratification. A scaling law for SAFT, incorporating the effective Lewis number to quantitatively characterize hydrogen's unique transport properties, is revised for stretched premixed laminar flames. Section 2.2 explores fundamental mechanisms of NO*x* formation and establishes an exponential relationship between NO*x* emission rates and SAFT. With the new insights of SAFT and fuel re-stratification, a novel concept based on the synergistic effect of fuel stratification and preferential diffusion is proposed in Section 3 for achieving ultra-low NO*x* emissions in hydrogen combustion. The effectiveness of this concept is subsequently demonstrated using a representative multi-slot configuration, highlighting its potential for practical application in low-emission hydrogen combustion systems.

2. Hydrogen chemical and transport characteristics

2.1. SAFT and fuel re-stratification

For traditional fuels like methane, transport properties are often simplified using the unity-Lewis number assumption, under which thermal and mass diffusivity are considered equal. However, this approximation is not applicable to hydrogen-air mixtures, in which the Lewis number deviates significantly from unity. Such disparities in transport properties give rise to distinct flame behaviors, including altered flame temperature and species distributions, which can strongly influence practical flame configurations. Consequently, a fundamental understanding of hydrogen flame characteristics—particularly SAFT and fuel re-stratification—is critical for the development of carbon-free energy and propulsion systems.

In this study, transport properties are characterized using the effective Lewis number (Le_{eff}), which is calculated for fuel/air mixtures as follows [21]:

$$\mathrm{Le}_{\mathrm{eff}} = 1 + \frac{Le_{\mathrm{E}} - 1 + A(Le_{\mathrm{D}} - 1)}{1 + A} \quad (1)$$

where Le_{E} and Le_{D} denote the Lewis number of the reactant in excess and deficiency, respectively. The parameter $A = 1 + Ze(1/\Phi - 1)$ quantifies the mixture strength, where Φ equals ϕ under lean conditions and $1/\phi$ under rich conditions. ϕ is the nonuniform equivalence ratio. The Zel'dovich number is defined as $Ze = E_{\mathrm{a}}(T_{\mathrm{ad}} - T_{\mathrm{u}})/(R^0 T_{\mathrm{ad}}^2)$, where R^0 is the universal gas constant, E_{a} is the global activation energy, T_{ad} is the adiabatic flame temperature, and T_{u} is the unburnt gas temperature. For off-stoichiometric conditions, E_{a} is determined following the methodology proposed by Law [22]: $E_a = -2R^0\left\{\frac{\mathrm{d}\ln(f^0)}{\mathrm{d}(1/T_{\mathrm{ad}})}\right\}_{\mathrm{p}}$, where f^0 denotes the mass burning rate, and p denotes the operating pressure. Near stoichiometric conditions, E_{a} is interpolated from the off-stoichiometric results, as recommended by Jomaas et al. [23].

The effective Lewis numbers for hydrogen-air mixtures at different equivalence ratios are presented in Fig. 1(a). At rich conditions, Le_{eff} exceeds unity due to the high thermal diffusivity of H_2 at standard conditions ($1.4 \times 10^{-4}\ \mathrm{m}^2 \cdot \mathrm{s}^{-1}$), which significantly increases the thermal diffusivity of the premixed mixture compared to the mass diffusivity of oxygen in nitrogen ($1.9 \times 10^{-5}\ \mathrm{m}^2 \cdot \mathrm{s}^{-1}$). In contrast, at lean conditions, Le_{eff} falls below unity because the mass diffusivity of hydrogen in nitrogen ($7.1 \times 10^{-5}\ \mathrm{m}^2 \cdot \mathrm{s}^{-1}$) exceeds the thermal diffusivity of air ($2.0 \times 10^{-5}\ \mathrm{m}^2 \cdot \mathrm{s}^{-1}$). The hydrogen relevant mass diffusivity and thermal diffusivity are taken from Ref. [24]. This behavior is markedly different from that of hydrocarbon fuels. For methane-air mixtures, Le_{eff} remains close to unity across all equivalence ratios. This behavior arises because, at standard conditions, the mass diffusivity of methane in nitrogen ($2.1 \times 10^{-5}\ \mathrm{m}^2 \cdot \mathrm{s}^{-1}$) is similar to that of oxygen in nitrogen ($1.9 \times 10^{-5}\ \mathrm{m}^2 \cdot \mathrm{s}^{-1}$), and the thermal diffusivity of methane (2.2×10^{-5}

remain of the same order of magnitude. In the case of n-dodecane, the effective Lewis number exhibits an opposite trends to hydrogen: Le_{eff} exceeds 2 under lean conditions but decreases below unity for equivalence ratios greater than 1.4.

The deviation of the effective Lewis number from unity leads to distinct flame behaviors, particularly in stretched flames, affecting flame temperature and flame speed. Taking an opposed adiabatic stagnation flame as an illustrative example, the temperature response of a stretched premixed flame ($\tilde{T}_{\mathrm{b}}$) has been derived in Ref. [15] as

$$\begin{cases} \tilde{T}_{\mathrm{b}} = 1 + \left(\frac{1}{Le} - 1\right)\frac{\tilde{\mathcal{K}}}{(\tilde{f}_{\mathrm{u}})^2} \\ \tilde{f}_{\mathrm{u}} = \frac{1}{\tilde{\delta}_T} = \exp\left[\frac{Ze}{2}(\tilde{T}_{\mathrm{b}} - 1)\right] \end{cases} \quad (2)$$

where the dimensionless parameter $\tilde{T}_{\mathrm{b}} = (T_{\mathrm{b}} - T_{\mathrm{u}})/(T_{\mathrm{ad}} - T_{\mathrm{u}})$, $\tilde{\mathcal{K}} = \kappa\delta_T^0/s_{\mathrm{u}}^0$ where δ_T^0 is the flame thickness in unstretched flames, s_{u}^0 is the laminar flame velocity in unstretched flames, and κ is the flame stretch rate and defined as

$$\kappa = \frac{1}{A}\cdot\frac{\mathrm{d}A}{\mathrm{d}t} \quad (3)$$

To illustrate the significance of the Lewis number, Fig. 1(b) presents the maximum flame temperature ($\mathrm{T}_{\mathrm{max}}$) as a function of stretch rates in laminar premixed opposed flames for different fuels. Hydrogen with an equivalence ratio of 0.4, methane with an equivalence ratio of 0.5, and n-dodecane with an equivalence ratio of 0.8 are selected to represent fuels with effective Lewis numbers less than unity, approximately unity, and greater than unity, respectively. The results demonstrate that the maximum flame temperature exceeds, remains close to, or falls below the adiabatic flame temperature as the effective Lewis number decreases from greater than one to less than one. Specifically, flames with a Lewis number less than one exhibit SAFT, while those with a Lewis number greater than one show sub-adiabatic behavior. With further increases in stretch rate, all flames eventually extinguish as a result of reduced residence time.

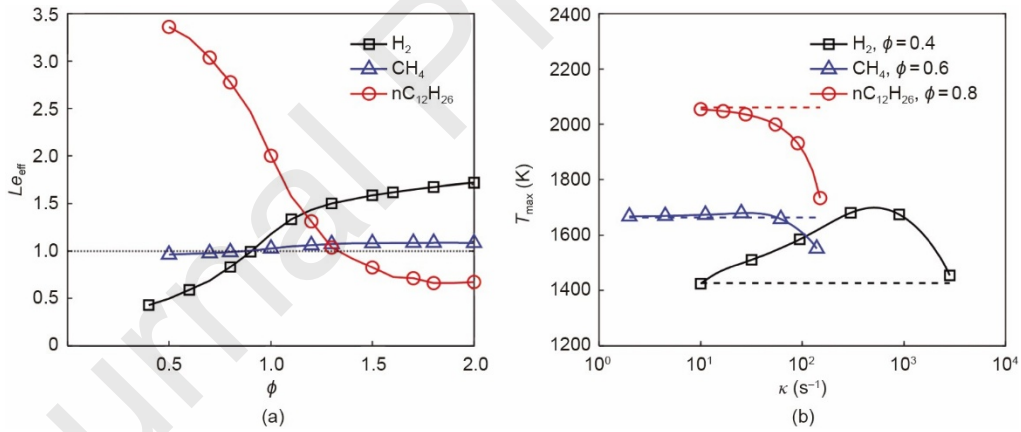

Fig. 1. (a) Effective Lewis numbers with equivalence ratio and (b) the maximum flame temperature (T_{max}) with strain rate for H_2. Also shown are the values of CH_4 and $nC_{12}H_{26}$ for comparison.

To further explore SAFT in lean premixed hydrogen combustion, Fig. 2 presents contours of temperature and local equivalence ratio as functions of axial distance and stretch rates for an opposed laminar flame with a global equivalence ratio of $\phi = 0.4$. As the stretch rate increases, the flame surfaces progressively move toward the stagnation plane and eventually extinguish. To quantify the effect of a low Lewis number, the local equivalence ratio ϕ_{local} is defined as

$$\phi_{\mathrm{local}} = \frac{x_{\mathrm{H,\,local}}/x_{\mathrm{O,\,local}}}{x_{\mathrm{H,stoic}}/x_{\mathrm{O,stoic}}} \quad (4)$$

where x_{H} and x_{O} are the molar fraction of H and O, and the subscripts 'local' and 'stoic' refer to local and stoichiometric conditions. The results show that the local equivalence ratio decreases sharply across the flame front and increases in the product zone, indicating preferential transport of hydrogen from the preheat zone to the product zone. Furthermore, as the stretch rate increases, ϕ_{local} in the product zone rises monotonically from the global equivalence ratio of 0.4 to values exceeding 0.6. A Lewis number below unity implies that mass diffusivity exceeds thermal diffusivity, resulting in an imbalance in between species and heat transport. This imbalance leads to elevated flame

Journal Pre-proofs

temperatures in the product zone. Specifically, the maximum flame temperature exceeds 1600 K at stretch rates above [illegible] to incomplete chemical reactions associated with reduced residence time. In stretched flames, the reduced flame thickness further amplifies these effects, causing more chemical energy to diffuse toward the burned side while less heat diffuses toward the unburned side. This imbalance ultimately results in SAFT and fuel re-stratification.

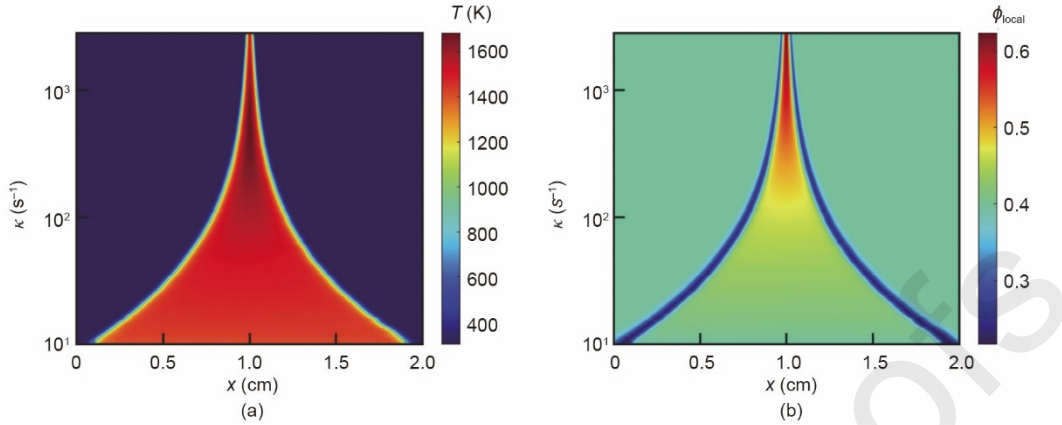

Fig. 2. Contours of (a) temperature and (b) local equivalence ratio in opposed premixed hydrogen flames under different strain rates for the case of $\phi = 0.4$, $p = 1$ atm (1 atm = 101.325 kPa), and $T_u = 298$ K, x denotes local spatial coordinate

*2.2. The dependence of NO*x *on flame temperature*

NOx formation is strongly governed by chemical kinetics. The underlying reaction pathways are dominated by chain-branching and chain-termination mechanisms within the H_2/O_2 system. The key elementary reactions are summarized below.

Chain-branching:

$$H + O_2 \rightarrow O + OH \quad (H1)$$

$$O + H_2 \rightarrow H + OH \quad (H2)$$

$$H_2 + OH \rightarrow H_2O + H \quad (H3)$$

$$O + H_2O \rightarrow OH + OH \quad (H4)$$

Chain-termination:

$$H + H + M \rightarrow H_2 + M \quad (H5)$$

$$O + O + M \rightarrow O_2 + M \quad (H6)$$

$$H + O + M \rightarrow OH + M \quad (H7)$$

$$H + OH + M \rightarrow H_2O + M \quad (H8)$$

$$H + O_2 + M \rightarrow HO_2 + M \quad (H9)$$

As widely documented in the literature [25], the H_2/O_2 system is highly sensitive to the key chain-branching reaction (H1) and the critical chain-termination reaction (H9). Two important phenomenological parameters for characterizing flames behavior are the adiabatic flame temperature and laminar flame speed. Fig. 3 compares these quantities for hydrogen, methane, and n-dodecane at pressure ratios of 1 and 20. The unburnt gas temperature and operating pressure are related through the isentropic compression relation:

$$\frac{T}{T_0} = \left(\frac{P}{P_0}\right)^{\frac{\gamma-1}{\gamma}} \quad (5)$$

where $T_0 = 298$ K and $P_0 = 1$ atm denote standard conditions, $\gamma = 1.4$ is the specific heat ratio. The results indicate that hydrogen has both a higher adiabatic flame temperature and an extremely higher laminar flame speed than

150 to 500 K as the equivalence ratio increases from 0.5 to 2. The laminar flame speed at stoichiometric equivalence ratio of hydrogen is approximately five times that of hydrocarbon fuel, with its maximum values occurring at an equivalence ratio of about 1.8. These pronounced differences in adiabatic flame temperature and laminar flame speed have significant effects on NO*x* emissions and risk of flashback during the transition from hydrocarbon-fueled burners to hydrogen-fueled burners. Consequently, elucidating the impact of SAFT on NO*x* formation is of critical practical importance for the development of low-NO*x* hydrogen-fueled combustion systems.

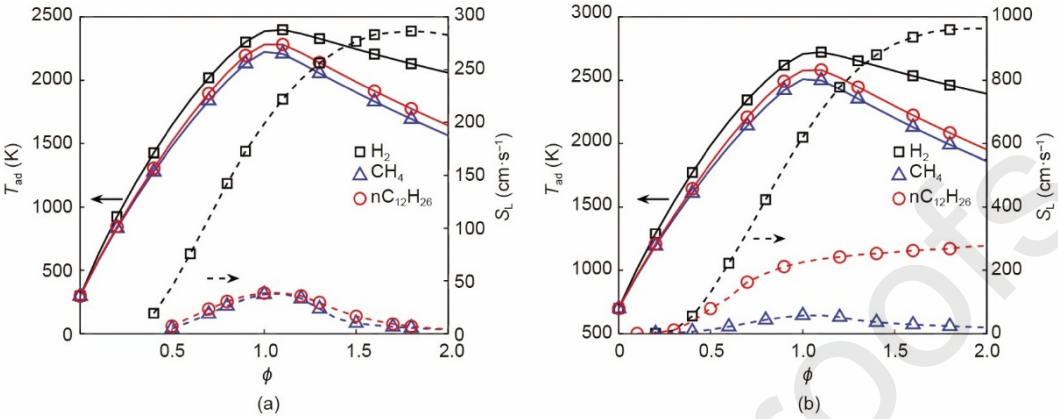

Fig. 3. The variation of adiabatic flame temperature (T_{ad}) and laminar flame speed (S_L) with equivalence ratio for hydrogen at pressure ratio of (a) 1 and (b) 20. Also shown are values of CH_4 and $nC_{12}H_{26}$ for comparison.

The formation of nitrogen oxides (NO and NO_2) in combustion involves a large number of elementary reactions [26]. In most combustion systems, nitric oxide (NO) is the dominant nitrogen oxide species, and its formation primarily proceeds through three pathways: the thermal route, the N_2O route, and the NNH route [27].

The thermal NO mechanism consists of three elementary reactions:

$$N_2 + O \rightarrow NO + \quad (R1)$$

$$O_2 + N \rightarrow NO + \quad (R2)$$

$$N + OH \rightarrow NO + \quad (R3)$$

This reaction sequence is known as the Zel'dovich mechanism. The rate-controlling reaction is Reaction (R1), which involves the dissociation of the tight N_2 triple bond and therefore becomes significant only at elevated temperature. Under the steady-state assumption for atomic nitrogen, the thermal NO formation rate can be approximated as [28]

$$\omega_{NO,thermal} \sim \frac{k_1[N_2][O]}{\rho} \sim k_1[O] \sim k_1 k_p [O_2]^{1/2} \quad (6)$$

where k_1 is the temperature-dependent rate constant of Reaction (R1), $[N_2]$, [O], and $[O_2]$ are molar concentrations of nitrogen, atomic oxygen, and molecular oxygen, respectively, ρ is the mixture density, and k_p is the temperature-dependent equilibrium constant. Thermal NO formation is highly sensitive on temperature and largely independent of fuel type. Owing to the strong temperature dependence of k_1, the thermal NO production rate approximately doubles for every 90 K temperature increase above 2200 K.

The N_2O pathway requires a third molecular M to exist. The main elementary reactions are as follows:

$$N_2 + O + M \rightarrow N_2O + \quad (R4)$$

$$N_2O + O \rightarrow 2NO \quad (R5)$$

$$N_2O + H \rightarrow NO + \quad (R6)$$

The NNH route was discovered in 1995 [29] and its essential reactions are:

$$N_2 + H \rightarrow NNH \quad (R7)$$

$$\mathrm{NNH + O \rightarrow NO + H (R8)}$$

In addition, the NNH route and the N_2O route are linked by the reaction

$$\mathrm{NNH + O \rightarrow N_2O + H (R9)}$$

Fig. 4 shows the profiles of temperature, NO mass fraction, thermal NO mass fraction, and non-thermal NO mass fraction against the residence time in one-dimensional free-propagating premixed hydrogen flame with an equivalence ratio of 0.60. The unburnt gas temperature is 298 K, and the pressure is atmospheric. The residence time t^* is defined as:

$$t^* = \int_{x_0}^{x} \frac{1}{u(x)} \mathrm{d}x \quad (7)$$

where x and u denote local spatial coordinate and flow velocity, respectively. The subscript 0 refers to the flame front location, which is defined as the position where hydrogen conversion rate equals 0.95. The hydrogen conversion rate α_{H} is defined as the mole ratio between H-atom in H_2O and total H-atom in the mixture:

$$\alpha_{\mathrm{H}} = \frac{2X_{\mathrm{H_2O}}}{\sum_k n_k X_k} \quad (8)$$

where X_k and n_k represent the mole fraction and number of H-atom of kth species. $X_{\mathrm{H_2O}}$ denotes the mole fraction of H_2O. It is shown that the NO profile exhibits two distinct regimes: a rapid increase near the flame front, followed by an approximately linear growth in the post-flame zone. In the latter region, the temperature approaches the adiabatic flame temperature and thermal NO formation becomes the dominant formation pathway.

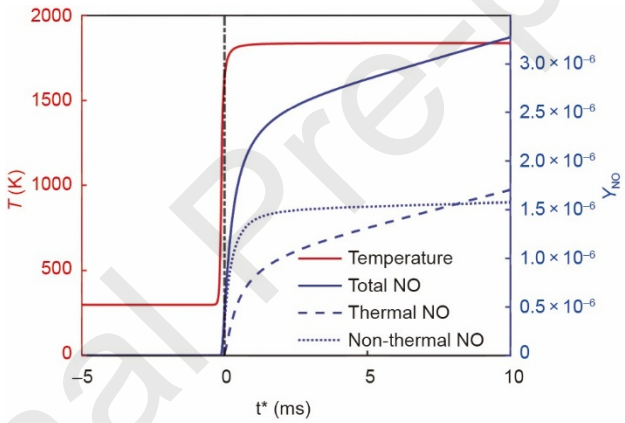

Fig. 4. NO formed from thermal and non-thermal route in one-dimensional hydrogen premixed flame of $p = 1$ atm, $T_{\mathrm{u}} = 298$ K, $\phi = 0.60$. T and Y_{NO} represent temperature and mass fraction of NO, respectively.

Fig. 5 depicts the relative contribution of thermal and non-thermal NO formation pathways in free-propagating laminar hydrogen flames at a representative residence time of 10 ms. NO formation is dominated by the thermal NO route with a temperature higher than 1800 K. For instance, at a pressure ratio of 1 and an equivalence ratio of 0.60, corresponding to an adiabatic flame temperature of 1838 K, the thermal route accounts for 52% of the total NO formation. At a pressure ratio of 20, the elevated adiabatic flame temperature leads to an increase in total NO emissions by two orders of magnitude (approximately 288-fold), with the thermal route contributing more than 85%. In addition, non-thermal NO formation also exhibits strong temperature dependence. These results highlight that effective reduction of local flame temperature is critical for achieving low NO*x* emissions in hydrogen combustion systems.

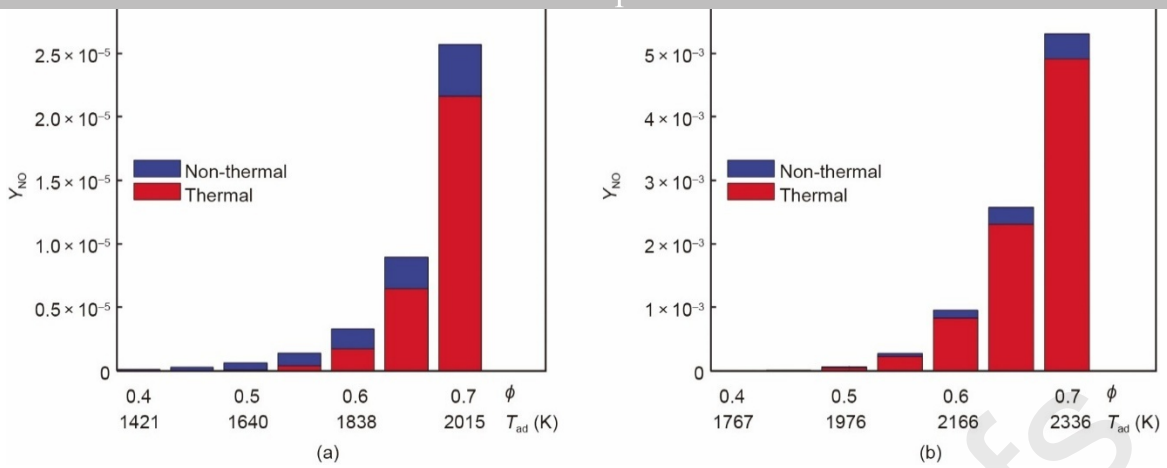

Fig. 5. NO formed from thermal and non-thermal routes in one-dimensional hydrogen premixed flames with a pressure ratio of (a) 1 and (b) 20.

To quantify the effect of SAFT on NO emissions, an experience expression for the thermal NO formation rate, based on the equilibrium model for [O] is expressed as [30,31]

$$\frac{\mathrm{d[NO]}}{\mathrm{d}t} \approx 1.43 \times 10^{14} T^{-\frac{1}{2}} \mathrm{e}^{-\frac{69460}{T}} [\mathrm{O_2}]^{\frac{1}{2}} [\mathrm{N_2}] \quad (9)$$

where T is the temperature.Assuming a SAFT of the form $T_\mathrm{b} = T_\mathrm{ad}(1+\epsilon)$, where ϵ is a small quantity, the ratio of the thermal NO reaction rate at SAFT to that at adiabatic flame temperature can be written as:

$$\frac{(\mathrm{d[NO]}/\mathrm{d}t)_\mathrm{b}}{(\mathrm{d[NO]}/\mathrm{d}t)_\mathrm{b}^0} = (1+\epsilon)^{-\frac{1}{2}} \mathrm{e}^{\frac{A_0\epsilon}{1+\epsilon}} \quad (10)$$

where the exponential factor $A_0 = 69460/T_\mathrm{ad}$, which is approximately 35 for lean hydrogen combustion. Retaining only the first-order term in ϵ, Eq. (10) reduces to

$$\frac{(\mathrm{d[NO]}/\mathrm{d}t)_\mathrm{b}}{(\mathrm{d[NO]}/\mathrm{d}t)_\mathrm{b}^0} \approx \mathrm{e}^{A_0\epsilon} \quad (11)$$

This equation demonstrates that thermal NO formation is highly sensitive to ϵ. For laminar premixed opposed flames, the relationship between SAFT and stretch rate can be obtained from Eq. (2):

$$T_\mathrm{b} = T_\mathrm{u} + (T_\mathrm{ad} - T_\mathrm{u}) \cdot \left(1 + \frac{1}{Ze} W\left(Ze \cdot \tilde{\mathcal{K}}\left[\frac{1}{Le} - 1\right]\right)\right) \quad (12)$$

where $W(\cdot)$ presents the Lambert W-function. Taking $\tilde{\mathcal{K}} = 1$, the super-adiabatic temperature increment ϵ is estimated to be 0.12 at an equivalence ratio of 0.55, yielding an amplification factor of approximately 67 for thermal NO formation. The flame temperature declines toward the adiabatic value along the flow direction, leading to a reduction in the amplification factor. Assuming a linear temperature decay, the spatially averaged amplification factor remains on the order of several times the NO values without SAFT. These findings suggest that fully premixed hydrogen combustion does not achieve the optimal low NO*x* emission for hydrogen. Instead, a new combustion technology with fuel stratification is required to mitigate SAFT and fuel re-stratification, thereby effectively reducing NO emissions.

3. Synergistic effects of fuel stratification and preferential diffusion

NO*x* formation is highly sensitive to local flame temperature and equivalence ratio. Fully premixed lean combustion is widely recognized as an effective strategy for NO*x* reduction, as it generally results in a low and uniform temperature field. However, in hydrogen-enriched combustion, this conventional paradigm does not work well. The combined effects of preferential diffusion and flame stretching can lead to SAFT and fuel re-stratification. In addition, the Soret effect further promotes local accumulation of hydrogen in the high-temperature zones, thereby enhancing SAFT and fuel re-stratification. The role of the Soret effect has been previously investigated in an opposed laminar flame of lean premixed hydrogen ($\phi = 0.4$), as documented in Ref. [32]. These phenomena cause local temperature and equivalence ratio to exceed the adiabatic flame temperature and global equivalence ratio of a fully premixed system, thereby

Journal Pre-proofs

significantly enhancing NOx formation. To mitigate these adverse effects, fuel stratification is introduced as an effective [illegible]al equivalence ratio, fuel stratification counteracts preferential diffusion-induced enrichment in reaction and product zones. This controlled non-uniformity attenuates SAFT, suppresses local equivalence ratio peaks, and promotes a more uniform temperature profile, providing a promising pathway for suppressing NO*x* emissions in hydrogen-containing flames.

To demonstrate the effectiveness of the proposed fuel-stratified combustion technology, the multi-slot laminar flames (as illustrated in Fig. 6) are designed to mimic the flame-flame interactions in the micromixer configurations, which have attracted significant interest for low-emission hydrogen gas turbines [33,34]. In such configurations, flame fronts experience both positive stretch in the near field and negative stretch close to the flame tip. In the present multi-slot nozzle configuration, each slot has a width of 1 mm, with a 1 mm gas separating adjacent slots. The vertical distance from the slot exit to the outlet is 90 mm, while the distance from the inlet to the uppermost part of the slots is 3.6 mm. The rectangular computational domain is discretized into 36 000 quadrilateral cells, with local mesh refinement employed to resolve the near-wall regions and the jet. The domain extends 90 times the slot width in the downstream (y) direction and 3.6 times the slot width in the upstream direction.

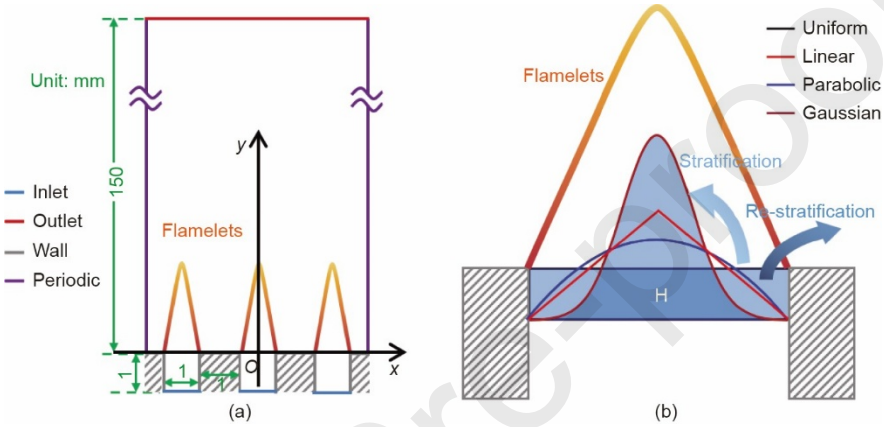

Fig. 6. The schematic diagrams of (a) multi-slot flame and (b) fuel stratification with different inlet ϕ-profiles.

The transport equations for species mass fractions Y_k yields

$$\frac{\partial \rho Y_k}{\partial t} + \frac{\partial}{\partial x_j}(\rho u_j Y_k) = \frac{\partial J_{jk}}{\partial x_j} + R_k \quad (13)$$

where ρ, u_j, and Y_k denote the density, velocity in the jth direction, and mass fraction of the kth species, respectively. x_j , The term J_{jk} represents the mass flux of species k in the jth direction, which arise from gradients of both concentration and temperature (Soret effect). The flux can be expressed as

$$J_{jk} = J_{jk,c} + \rho \frac{D_{T,k}}{T} \cdot \frac{\partial T}{\partial x_j} \quad (14)$$

where $D_{k,T}$ is the thermal diffusion coefficient adopted the following formulation [35]:

$$D_{k,T} = -2.59 \times 10^{-7} \times T^{0.659} \cdot \left(\frac{M_{w,k}^{0.511} X_k}{\sum_{i=1}^{N} M_{w,i}^{0.511} X_i} - Y_k \right) \cdot \frac{\sum_{i=1}^{N_s} M_{w,i}^{0.511} X_i}{\sum_{i=1}^{N_s} M_{w,i}^{0.489} X_i} \quad (15)$$

where $M_{w,i}$ and X_i denote the molecular weight and mole fraction of species i, respectively. N_s is the number of species. X_k denotes the mole fraction of species k. The diffusion flux arising from the gradient of concentration, $J_{jk,c}$, is modeled using full multicomponent model. In this approach, the diffusion flux derived from Maxwell-Stefan equations [36] can be expressed as

$$J_{jk,c} = \rho \sum_{l=1}^{N-1} D_{kl} \frac{\partial Y_l}{\partial x_j} \quad (16)$$

where $D_{kl} = [D]$ is a $(N-1) \times (N-1)$ diffusion coefficient matrix of generalized Fick's Law, which depends on species mole fraction, molecular weight, and binary mass diffusion coefficient among species in mixture. Y_l denotes the mass fraction of species l.

es over the N_R elementary reactions in which species k participates. The rth elementary reaction in a mixture with N_s species written in general form as follows:

$$\sum_{i=1}^{N_s} \nu'_{k,r}\mathcal{M}_k \underset{k_{b,r}}{\overset{k_{f,r}}{\rightleftharpoons}} \sum_{i=1}^{N_s} \nu''_{k,r}\mathcal{M}_k \quad (17)$$

where $\mathcal{M}_k$, $\nu'_{k,r}$, and $\nu''_{k,r}$ denotes species k, the stoichiometric coefficient of the reactant and product, respectively. The forward reaction rate constant $k_{f,r}$ follows the Arrhenius equation

$$k_{f,r} = A_r T^{\beta_r} e^{-E_{a,r}/RT} \quad (18)$$

where A_r is the pre-exponential factor, β_r is the temperature exponent, and $E_{a,r}$ is the activation energy of the rth reaction. The backward rate constant $k_{b,r}$ is obtained from the forward rate constant $k_{f,r}$ and the equilibrium constant K_r. By summing the contributions from all reactions, the chemical source term for kth species is expressed as

$$R_k = M_{w,k}\sum_{r=1}^{N_r}\left\{\left(\nu''_{k,r} - \nu'_{k,r}\right)\left(k_{f,r}\prod_{j=1}^{N_s}[c_j]^{\nu'_{j,r}} - k_{b,r}\prod_{j=1}^{N_s}[c_j]^{\nu''_{j,r}}\right)\right\} \quad (19)$$

where $[c_j]$ is the molar concentration of species j. $M_{w,k}$ denotes the molecular weight of species k which is the same as $M_{w,i}$ in essence, and N_r is the number of reactions. $\nu'_{j,r}$ and $\nu''_{j,r}$ denote the stoichiometric coefficient of species j in reactant and product, respectively which are the same as $\nu'_{k,r}$ and $\nu''_{k,r}$ in essence.

The continuity, momentum, and energy equations, coupled with chemical combustion kinetics were solved using a two-dimensional pressure-based solver under the incompressible ideal-gas assumption. Chemical kinetics were modeled using a kinetic mechanism for H_2-air combustion, consisting of 15 species and 47 elementary reactions and containing all major NOx pathways proposed by Capurso et al. [37]. Transport properties were evaluated using a mixture-average approach for viscosity and thermal diffusivity, while molecular diffusivity was derived from the multicomponent model. The specific heat capacity of the mixture was calculated using the mixing law.

The presence of SAFT and fuel re-stratification diminishes the low-emission advantages of premixed combustion, prompting interest in partially premixed combustion technologies. Building on the enrichment of hydrogen and temperature at the flame root caused by differential diffusion (as described in the previous section), a fuel stratification strategy is proposed to mitigate SAFT and fuel re-stratification, as shown in Fig. 6(b). This strategy involves distributing less fuel near the walls and more fuel at the center upstream of the combustion zone. Representative inlet equivalence ratio profiles are depicted in Fig. 6(b). Fig. 7 compares the temperature, local equivalence ratio, and mass fraction of NO between fully premixed flames and partially premixed flames employing different inlet ϕ-profiles. The results demonstrate that the bell-shaped ϕ-profile suppresses SAFT by approximately 100 K, reduces the peak local equivalence ratio by about 0.3, and lowers the NO mass fraction at the flame root by 2×10^{-6}, while maintaining the same outlet temperature. Although the absolute reduction in NO concentration for the present case appears modest, this approach clearly alleviates local SAFT, achieves a more uniform temperature distribution in the combustor, and reduces NO emissions at the outlet by 48% compared to fully premixed combustion. These findings verify the feasibility of the proposed combustion strategy, in which artificial fuel stratification mitigates fuel re-stratification and SAFT, ultimately lowering NOx emissions.

Journal Pre-proofs

Journal Pre-proofs

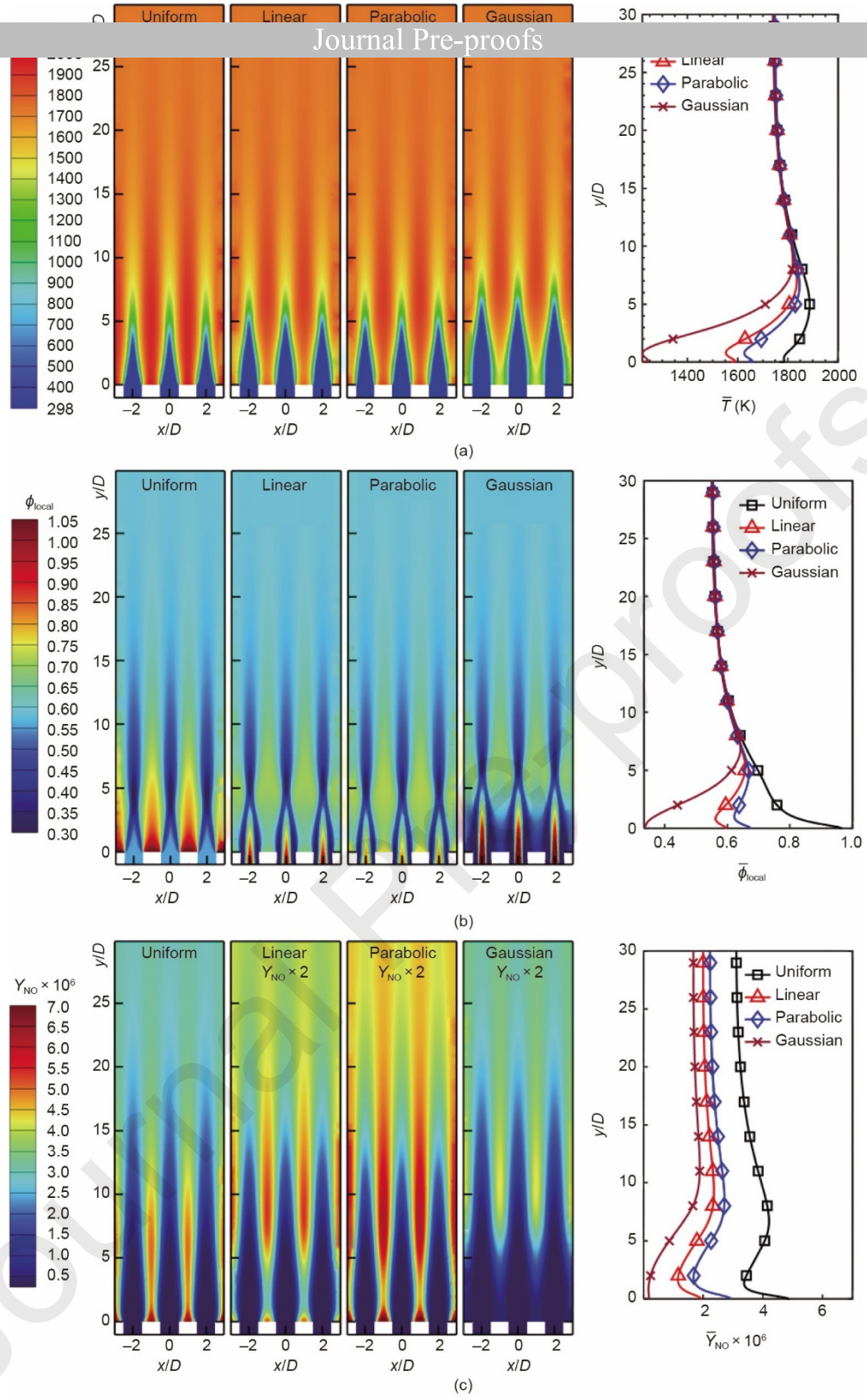

Fig. 7. Contours and horizontal averaged values within the main product zone (e.g., $x/D \in [0.5,1.5]$) along the y-axis for (a) temperature, (b) local equivalence ratio, and (c) NO mass fraction, using uniform, linear, parabolic, and Gaussian inlet ϕ-profile with a global equivalence ratio of 0.55. $\overline{T}$, $\overline{\phi}_{\text{local}}$ and $\overline{Y}_{\text{NO}}$ denotes the horizontal averaged temperature, local equivalence ratio and NO mass fraction within the main product zone (e.g., $x/D \in [0.5, 1.5]$) which is a function of *y/D*, respectively.

To further illustrate the manifestations of SAFT and fuel re-stratification, scatter plots of temperature versus local equivalence ratio ($T - \phi_{\text{local}}$) are presented in Fig. 8 for uniform, linear, parabolic, and Gaussian inlet ϕ-profiles. The black dashed and dotted lines denote the global equivalence ratio and corresponding adiabatic flame temperature, respectively, while the red solid line represents the adiabatic flame temperature across equivalence ratios. The uniform inlet exhibits pronounced SAFT and fuel re-stratification, as evidenced by the northeast cluster of scatter points, where temperatures exceed the corresponding adiabatic flame temperature by up to 240 K and local equivalence ratios surpass

parabolic, linear, and Gaussian inlet ϕ-profiles achieve peak temperatures of 1884, 1872, and 1855 K, respectively, and peak local equivalence ratios of 0.71, 0.66, and 0.65. Furthermore, the Gaussian ϕ-profile results in a greater concentration of scatter points in the low-temperature zone (southwest region), indicating a more uniform temperature field. These findings demonstrate that upstream fuel stratification—transferring more hydrogen away from stretched flame regions—effectively reduces peak temperatures and suppresses NO*x* formation.

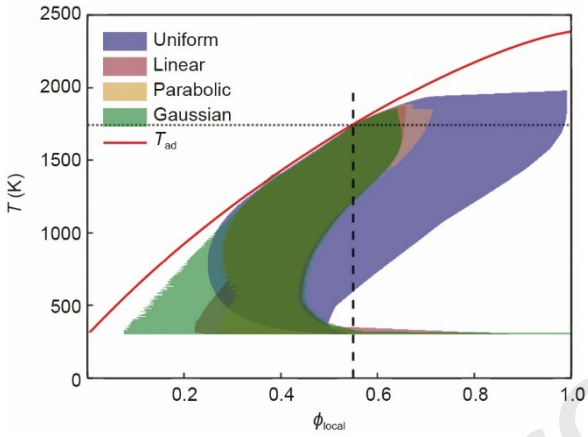

Fig. 8. Scatter plot of temperature and local equivalence ratio using uniform, linear, parabolic, and Gaussian inlet ϕ-profiles with a global equivalence ratio of 0.55.

The synergistic interaction between fuel stratification and preferential diffusion exhibits nonlinear characteristics, originating from the strong coupling between preferential diffusion intensity and local equivalence ratio. This coupling can be quantitatively characterized by the effective Lewis number, which varies with equivalence ratio as partially illustrated in Fig. 1(a). Since the local equivalence ratio is influenced by transport and diffusion processes, a complex feedback mechanism emerges. When the equivalence ratio deviates significantly from unity, preferential diffusion becomes dominant, significantly amplifying its impact on flame structure and NO*x* formation.

To systematically evaluate the effectiveness of fuel stratification under varied operating conditions, a series of numerical simulations was conducted over a range of global equivalence ratios $0.4 \leq \phi \leq 0.7$. As summarized in Fig. 9(a), all non-uniform inlet ϕ-profile—linear, parabolic, and Gaussian distributions—consistently reduce NO emissions compared to the conventional uniform fuel distribution. Among these profiles, the Gaussian-type profile exhibits the highest NO reduction performance, with emission reductions varying from 54% at $\phi = 0.4$ to 17% at $\phi = 0.7$. This trend correlates with the behavior of SAFT, as depicted in Fig. 9(b), where the maximum non-dimensional temperature ($\tilde{T}_{\max}$) decreases as the equivalence ratio approaches unity. The attenuation of SAFT under near-stoichiometric conditions leads to a corresponding reduction in the effectiveness of fuel stratification for NO mitigation. These findings confirm that non-uniform fuel injection is particularly effective under lean combustion regimes, where preferential diffusion effects are most pronounced. The applicability of fuel stratification for NO*x* reduction in practical burners is subject to further experimental validation and is planned for future investigation, especially under turbulent flow conditions.

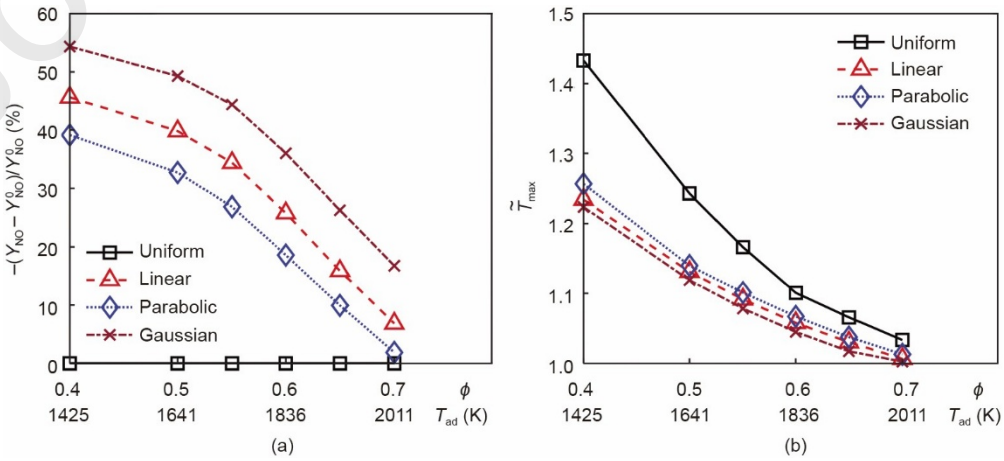

Fig. 9. (a) Maximum non-dimensional temperature and (b) NO reduction percentage relative to the uniform case for different inlet ϕ-

Journal Pre-proofs

mass fraction of outlet in the uniform case. Substituting Y_{NO}^{0} with $Y_{\mathrm{NO},0}$ is suggested to avoid ambiguity.

For practical applications involving elevated pressure and potentially intense turbulence, Fig. 5 indicates that elevated pressure substantially enhances NO formation, thereby amplifying the importance of fuel stratification strategies for effective NO*x* reduction. With respect to turbulence, while turbulent diffusion generally overwhelms molecular preferential diffusion in high-intensity turbulence, recent studies [32] have shown that preferential diffusion effects remain non-negligible. This is particularly relevant in the current multi-slot configuration, where flame stabilization occurs primarily within recirculation zones characterized by relatively weaker turbulent diffusion. As a result, the suppression of preferential diffusion by turbulence is less pronounced than conventionally assumed, suggesting that preferential diffusion maintains significant influence in practical micromixing burners. Consequently, fuel stratification is still expected to remain an effective strategy for achieving meaningful NOx reduction even under high-pressure turbulent operating conditions. In practical application, maintaining a designed fuel stratification profile under varying operational conditions requires a distributed fuel-air injection system equipped with active flow control. In such a configuration, a baseline stratification profile can be predefined for nominal operating points. During off-design operation, real-time regulation of the equivalence ratio distribution is achieved by dynamically adjusting fuel flow rates through individual injectors via control valves. This active fuel management strategy enables the system to adapt local mixture characteristics across different loads, thereby sustaining optimal combustion performance and low NO*x* emissions throughout the operational envelope. Such a control architecture provides a practical and scalable solution for gas turbine applications employing stratified combustion.

4. Conclusion

Hydrogen gas turbines represent a promising pathway toward decarbonized power generation; however, their combustion behavior differs fundamentally from that of natural gas systems due to hydrogen's distinctive transport properties. In particular, the low effective Lewis number of hydrogen under lean conditions induces SAFT and fuel re-stratification in stretched flames. These phenomena significantly enhance thermal NOx formation, thereby undermining the low-emission benefits typically associated with lean fully premixed combustion.

Numerical simulations of laminar hydrogen flames confirm the dominance of the thermal NO*x* route and reveal that SAFT can amplify local reaction rates by up to a factor of 67 relative to adiabatic conditions. Although spatial averaging moderates this amplification by several-fold, the results clearly illustrate the inherent limitations of conventional fully premixed combustion when applied to hydrogen. To address this challenge, a strategically designed fuel stratification approach is proposed. A systematic evaluation of various equivalence ratio profiles shows that non-uniform distributions—particularly a Gaussian-type ϕ profile—effectively reduce peak temperatures by 53-236 K and decrease NO emissions by 17% – 54% over the typical gas-turbine operating range of $0.4 < \phi < 0.7$, compared with a fully premixed configuration.

Future work will focus on developing generalized guidelines for optimal ϕ profiles, incorporating the effects of turbulent mixing, and experimentally validating NOx reduction performance. These efforts are expected to support the development of robust, ultra-low-NOx hydrogen combustion systems for practical gas turbine applications.

Acknowledgments

This work was supported by grants from the National Natural Science Foundation of China (52025062).

Compliance with ethics guidelines

Tianze Yu, Long Zhang, Hua Zhou, Zhuyin Ren, and Xiaohua Gan declare that they have no conflict of interest or financial conflicts to disclose.

References

[1] International Energy Agency. Net zero by 2050: a roadmap for the global energy sector. Report. Paris: International Energy Agency; 2021.

[2] Öberg S, Odenberger M, Johnsson F. Exploring the competitiveness of hydrogen-fueled gas turbines in future energy systems. Int J Hydrog Energy 2022;47(1):624–44.

[3] Zhou H, Xue J, Gao H, Ma N. Hydrogen-fueled gas turbines in future energy system. Int J Hydrog Energy 2024;64:569–82.

[4] Jiang J, Wan B, Yu T, Zhang L, Zhou H, Cai J, et al. Effects of structural variations on NO*x* formation in coaxial dual-swirl hydrogen flames. Int J Hydrogen Energy 2025;148:150047.

Aerosp Sci Technol 2025;162:110206.

[6] Berger L, Attili A, Gauding M, Pitsch H. LES combustion model for premixed turbulent hydrogen flames with thermodiffusive instabilities: a priori and a posteriori analysis. J Fluid Mech 2025;1003:A33.

[7] Wen X, Berger L, Cai L, Parente A, Pitsch H. Thermodiffusively unstable laminar hydrogen flame in a sufficiently large 3D computational domain–part I: characteristic patterns. Combust Flame 2024;263:113278.

[8] Rieth M, Gruber A, Williams FA, Chen JH. Enhanced burning rates in hydrogen-enriched turbulent premixed flames by diffusion of molecular and atomic hydrogen. Combust Flame 2022;239:111740.

[9] Wang X, Zhou H, Berger L, Pitsch H, Ren Z. Transported probability density function investigation on turbulent premixed hydrogen flames with thermodiffusive instability. AIAA J 2025;63(8):3445–60.

[10] Shi S, Schultheis R, Barlow RS, Geyer D, Dreizler A, Li T. Assessing turbulence–flame interaction of thermo-diffusive lean premixed H_2/air flames towards distributed burning regime. Combust Flame 2024;269:113699.

[11] Zhang X, Wang X, Zhou H, Ren Z. Effects of soret and differential diffusion on boundary layer flashback of H_2/CH_4 swirling flames. Proc Combust Inst 2024;40(1–4):105327.

[12] Zhang X, Chen Y, Liu J, Zhou H, Hou L, Ren Z. Laminar flame speed modeling of pre-vaporized jet fuel/hydrogen mixtures under engine conditions. Fuel 2025;380:133149.

[13] Matalon M, Matkowsky BJ. Flames as gasdynamic discontinuities. J Fluid Mech 1982;124:239–59.

[14] Chung SH, Law CK. An integral analysis of the structure and propagation of stretched premixed flames. Combust Flame 1988;72(3):325–36.

[15] Sun CJ, Law CK. On the nonlinear response of stretched premixed flames. Combust Flame 2000;121(1–2):236–48.

[16] Law CK, Sung CJ. Structure, aerodynamics, and geometry of premixed flamelets. Pror Energy Combust Sci 2000;26(4–6):459–505.

[17] Day MS, Bell JB, Gao X, Glarborg P. Numerical simulation of nitrogen oxide formation in lean premixed turbulent $H_2/O_2/N_2$ flames. Proc Combust Inst 2011;33(1):1591–9.

[18] Wen X, Berger L, Cai L, Parente A, Pitsch H. Thermodiffusively unstable laminar hydrogen flame in a sufficiently large 3D computational domain–part II: NO_x formation mechanism and flamelet modeling. Combust Flame 2024;265:113497.

[19] Vance FH, Scholtissek A. On the potential of using mixture stratification for reducing the flashback propensity of hydrogen flames. Appl Energy Combust Sci 2025;22100327.

[20] Lipatnikov AN. Stratified turbulent flames: recent advances in understanding the influence of mixture inhomogeneities on premixed combustion and modeling challenges. Pror Energy Combust Sci 2017;62:87–132.

[21] Bechtold JK, Matalon M. The dependence of the markstein length on stoichiometry. Combust Flame 2001;127(1–2):1906–13.

[22] Law CK. Propagation, structure, and limit phenomena of laminar flames at elevated pressures. Combust Sci Technol 2006;178(1–3):335–60.

[23] Jomaas G, Law CK, Bechtold JK. On transition to cellularity in expanding spherical flames. J Fluid Mech 2007;583:1–26.

[24] Ghajar A, Cengel Y. Heat and mass transfer: fundamentals and applications. 6th ed. New York City: Mcgraw-Hill Education; 2020.

[25] Li J, Zhao Z, Kazakov A, Dryer FL. An updated comprehensive kinetic model of hydrogen combustion. Int J Chem Kinet 2004;36(10):566–75.

[26] Miller JA, Bowman CT. Mechanism and modeling of nitrogen chemistry in combustion. Pror Energy Combust Sci 1989;15(4):287–338.

[27] Konnov AA, Colson G, De Ruyck J. NO formation rates for hydrogen combustion in stirred reactors. Fuel 2001;80(1):49–65.

[28] Rutar T, Malte PC. NO_x formation in high-pressure jet-stirred reactors with significance to lean-premixed combustion turbines. J Eng Gas Turbine Power 2002;124(4):776–83.

[29] Bozzelli J W, Dean AM. O + NNH: a possible new route for NO*x* formation in flames. Int J Chem Kinet 1995;27(11):1097–109.

[30] Hanson RK, Salimian S. Survey of rate constants in the N/H/O system. In: Gardiner WC, editor. Combustion chemistry. New York City: Springer; 1984. p. 361–421.

[31] Westenberg AA. Kinetics of NO and CO in lean, premixed hydrocarbon-air flames. Combust Sci Technol 1971;4(1):59–64.

[32] Yu T, Wang X, Zhang X, Zhou H, Ren Z. Numerical investigation of super-adiabatic flame temperature in multislot turbulent premixed l
Journal Pre-proofs

[33] Babazzi G, Gauthier PQ, Agarwal P, McClure J, Sethi V. NO_x emissions predictions for a hydrogen micromix combustion system. In: Proceedings of the ASME Turbo Expo 2019: Turbomachinery Technical Conference and Exposition; 2019 Jun 17–21; Phoenix, AZ, USA. New York City: ASME; 2019. p. V003T03A008.

[34] Haj Ayed A, Kusterer K, Funke HHW, Keinz J, Striegan C, Bohn D. Improvement study for the dry-low-NO_x hydrogen micromix combustion technology. Propuls Power Res 2015;4(3):132–40.

[35] Kuo KK. Principles of combustion. Hoboken: Wiley; 1986.

[36] Merk HJ. The macroscopic equations for simultaneous heat and mass transfer in isotropic, continuous and closed systems. Appl Sci Res 1959;8(1):73–99.

[37] Capurso T, Laera D, Riber E, Cuenot B. NO_x pathways in lean partially premixed swirling H2–air turbulent flame. Combust Flame 2023;248:112581.

Journal Pre-proofs

Declaration of Interest Statement

☒ The authors declare that they have no known competing financial interests or personal relationships that could have appeared to influence the work reported in this paper.

☐ The author is an Editorial Board Member/Editor-in-Chief/Associate Editor/Guest Editor for this journal and was not involved in the editorial review or the decision to publish this article.

☐ The authors declare the following financial interests/personal relationships which may be considered as potential competing interests:

Journal Pre-proofs